WIND TUNNEL EXPERIMENTS AND NUMERICAL SIMULATIONS ABOUT THE FLOW AND CONCENTRATION FIELDS AROUND TWIN HIGH-RISE BUILDINGS WITH A DISTRICT HEATING PLANT

Masaaki Ohba*, W. H. Snyder**, R. E. Lawson, Jr***, A. Huber****

ABSTRACT

This report describes the results of wind tunnel experiments and numerical simulations about the flow and concentration fields around twin high-rise buildings. These experiments and simulations were conducted at Environmental Protection Agency during Dr. Ohba's tenure from April in 1992 through March in 1993 as a visiting scientist.

From the wind tunnel experiments, it was found that, provided the twin high-rise building models were located such that the separation distance between the twin building models were longer than a building height, then upwind building would reduce the effects on the flow fields near the top of the downwind building model, and the separation distance would not substantially affect the magnitude of the downwind surface concentration contours for the downwind building.

The numerical simulations based on a k-ε model were conducted about three basic types of high-rise buildings using a CRAY supercomputer in EPA. Comparing the simulated results with experimental data for twin high-rise building models, the velocities along the upwind face of the downwind high-rise building model were predicted a little stronger than those in experimental data. Therefore, the reverse flow was not as clearly defined as that in the wind tunnel experiments. The overal good agreement with the wind tunnel data was achieved. However, for a single high-rise building model, the concentrations on the downwind surface were predicted higher than those for the twin high-rise buildings because the wake length was predicted longer than those for the twin building models. It is thought that our k-ε model needs to improve the accuracy of prediction.

1. INTRODUCTION

Recently in Japan, many high-rise office buildings have been built in downtown areas in order to effectively redevelop commercial districts. Many of these buildings have often

1993年10月6日受理

* 東京工芸大学建築学科教授
** U. S. Environmental Protecton Agency Air Resources 研究所部長
*** 同　上　研究員
**** 同　上　Atmospheric Research & Exposure Assessnent 研究所部長

been designed to have two high-rise structures atop a common, terrace-shaped lower level. Typically, as many as 5000 people might work in these buildings each day. As a result, the heat gain/loss inside the buildings is so great that district heating plants are necessary in order to provide building air conditioning for maintaining a comfortable working environment. If these district heating plants were installed near the high-rise buildings, they would generally be installed in the lower levels of the terrace section, and the exhaust would be vented on top of the terrace section near the base of the high-rise towers. Co-generation systems, widely used for district heating plants, emit large amounts of NO_x so that they may contribute significantly to increases in air pollution around the buildings. Therefore, the wind tunnel experiments and numerical simulations were designed to investigate the effects of three basic high-rise building configurations on the diffusion of emissions released near the downstream base of the high-rise structures.

2. EXPERIMENTAL DETAILS OF WIND TUNNEL EXPERIMENTS

2.1 WIND TUNNEL

The experiments were carried out in the wind tunnel of the U.S. Environmental Protection Agency's Fluid Modeling Facility (Snyder, 1979). The wind tunnel as shown in Figure 1 is of the open-return type with a test section 3.7 m wide, 2.1 m high and 18.3 m long. Figure 2 shows the vertical profiles of approach flow. A combination of spires (Irwin, 1981) and surface roughness was used to produce a thick simulated atmospheric boundary layer with a power-law index of 0.29, representative of well-developed downtown areas.

2.2 BUILDING MODELS

The high-rise building models were rectangular blocks with heights of 300, 450, 600 and 1200 mm(H_b), respectively. The building width and length were fixed at 200 mm. These corresponded to full-scale dimensions of 75, 112.5, 150 and 300 m, respectively, consistent with a scale ratio of 250 : 1. The terrace-shaped building model was 150 mm high, 1000 mm wide and 1400 mm long, corresponding to full-scale dimensions of 37.5 m×250 m×350 m. Figure 3 shows the layout of the twin building models.

2.3 EXPERIMENTAL CONDITIONS

Table 1 shows the range of experimental conditions for concentration measurements. The reference velocity (U_0) was kept at 3.5 m/s

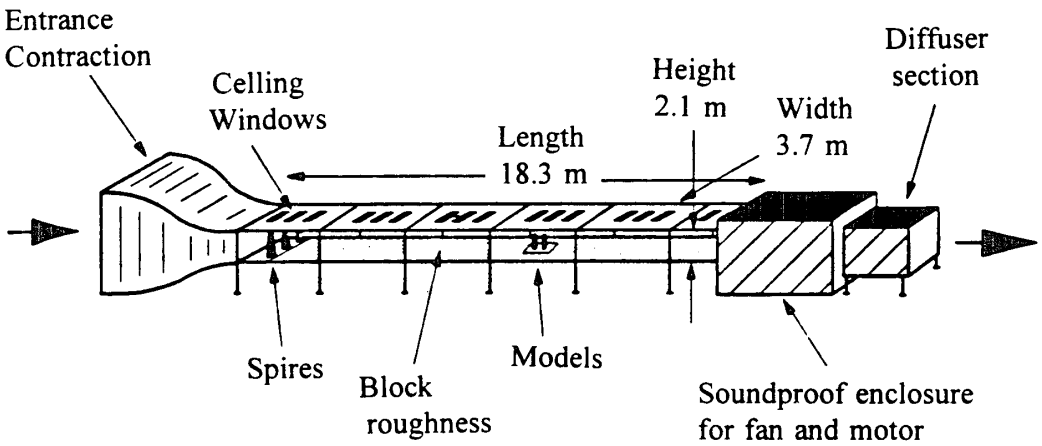

Figure 1. EPA meteorogical wind tunnel

at a position of X=0 mm and Z=600 mm.

(1) VELOCITY MEASUREMENTS

For Case 1, the center of the isolated building model was located 11.37 m downstream of the leading edge of the spires and along the longitudinal centerline of the tunnel. The U-W components at Y=0 mm and U-V components at Z=50 mm around the building model were measured using the pulsed wire anemometer. The U, V and W are mean velocity components in Cartesian coordinate. The twin high-rise building models for Case 2 where a second high-rise building model was set adjacent to the model of Case 1. The ratio of separation distance between building models to the building height (L/H_b) was 0.50. For Case 3, the twin high-rise building models on top of the terrace-shaped basement with the building height and separation height and separation distance are the same as for Case 2. For Case 4 through Case 6, L/H_b was equal to 0.25, 0.75 and 1.00, respectively, and U-W components were measured downstream of the downwind building model. For Case 7 through Case 16, U components were measured near ground level behind the downwind building model in order to determine the reattachment length behind the downwind building model.

(2) CONCENTRATION MEASUREMENTS

Source positions were restricted to locations in the downwind wake of the downwind build-

Table 1. Experimental conditions

Case Number	Bldgs location b1	b2	b3	b4	b5	Bldg height H_b [m]	Bldg distance L/H_b
1	0.60	0.250				0.60	0.00
2	0.60	0.250	0.60	−0.250	0.00	0.60	0.50
3	0.45	0.250	0.45	−0.250	0.15	0.60	0.50
4	0.45	0.175	0.45	−0.175	0.15	0.60	0.25
5	0.45	0.325	0.45	−0.325	0.15	0.60	0.25
6	0.45	0.400	0.45	−0.400	0.15	0.60	1.00
7	0.30	0.138	0.30	−0.258	0.00	0.30	0.25
8	0.30	0.175	0.30	−0.175	0.00	0.30	0.50
9	0.30	0.213	0.30	−0.213	0.00	0.30	0.75
10	0.30	0.250	0.30	−0.250	0.00	0.30	1.00
11	0.60	0.175	0.60	−0.175	0.00	0.60	0.25
12	0.60	0.325	0.60	−0.225	0.00	0.60	0.75
13	0.60	0.400	0.60	−0.400	0.00	0.60	1.00
14	1.20	0.250	1.20	−0.250	0.00	1.20	0.25
15	1.20	0.400	1.20	−0.400	0.00	1.20	0.50
16	1.20	0.550	1.20	−0.550	0.00	1.20	0.75

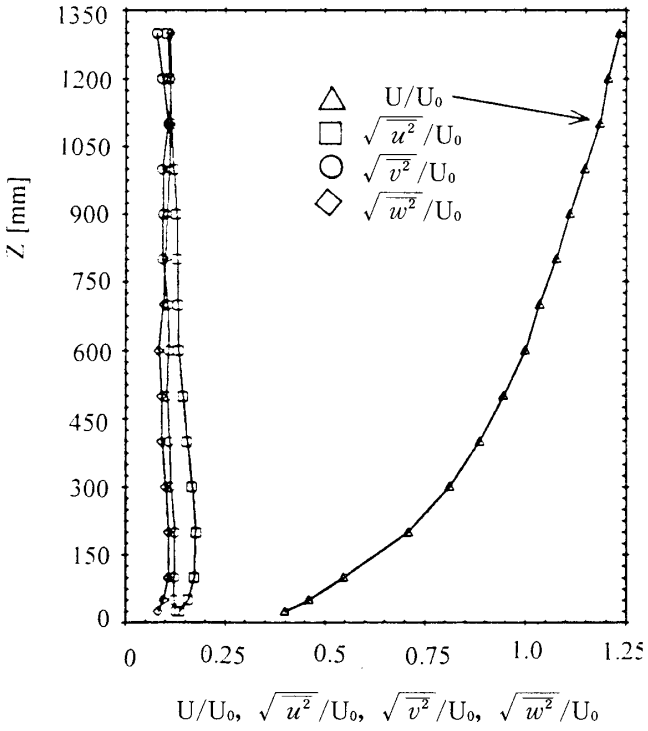

Figure 2. Vertical profiles of approach flow

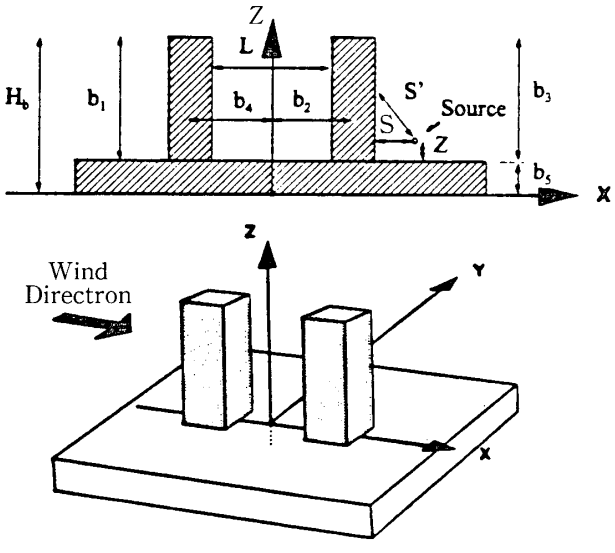

Figure 3. Schematic diagram of building models

ing model because the district heating plants are generally installed in an underground level and significant air pollution is expected to occur only in the building wake. The source heights were 25, 50 and 100 mm above either the tunnel floor or above the top surface of the terrace level. Primary source positions were at S=50, 100 and 150 mm from the downwind face of the building. Full surface concentration profiles were measured with each of these source heights and location for Case 1 through 6 and for Case 11 through 13. Abbreviated surface profiles, sufficient to determine the value and location of the maximum surface concentration were measured for Case 7, Case 10, Case 14 and Case 16. Measurements for Case 8, Case 9, Case 12 and Case 15 were not conducted because these concentration profiles were expected to be the same as those measured in adjacent experimental conditions. Lateral concentration profiles and ground-level concentration were not measured.

2.4 MEASUREMENT PROCEDURES

(1) VELOCITY MEASUREMENTS

A pulsed-wire anemometer was used for velocity measurements. The probes were traversed about the test section of the wind tunnel using an automated carriage. This system was controlled by the IBM compatible data acquisition microcomputer through the use of the FMF software program HOT. Positioning accuracy of the system was ±1 mm. All velocities were normalized by the reference velocity of 3.5 m/s.

(2) CONCENTRATION MEASUREMENTS

Ethane was used as a tracer gas and was emitted from the source at a flow rate of 1465 cc/min. The source was a hollow, perforated plastic sphere with a diameter of 10 mm. This simulated a point source and injected the tracer with negligible momentum in any one direction. The source was located in the recirculating wake downstream of the building. For building surface concentrations, samples of the dispersed plume were withdrawn through sampling ports on the building surface. Concentration measurements in the vertical center plane downstream of the buildings were obtained by using a rake of 6 ports that was fastened to a movable instrument carriage. The samples were routed from the rake or surface ports to a bank of hydrocarbon analyzers (flame ionization detectors) which provided an output voltage directly related to concentration. A sampling time of 120 seconds was used for all concentration measurements. All concentrations are presented in nondimensional form

$$\chi = CU_0H_b^2/Q$$

where C is the measured concentration in percent ethane, U_0 is wind speed at a height of 600 mm, H_b is the building height of 600 mm and Q is the tracer flow rate.

2.5 MEASUREMENT POINTS

(1) VELOCITY MEASUREMENTS

For the measurement of vertical profiles of Case 1, there were 188 measuring points, among which 46 points were located upstream of the isolated building model, 18 points were above the rooftop, and 124 points were downstream of the model. The points were distributed densely near the model. For Case 2 and Case 3, a total of 316 points and 278 points, respectively, were distributed around the twin building models. For the measurement of horizontal velocity profiles, the points were located at a height of 50 mm above the floor or terrace -shaped rooftop. The total number of points for Case 1, Case 2 and Case 3 were 128, 180 and 180, respectively.

(2) CONCENTRATION MEASUREMENTS

For measurement of building surface concentration with $H_b=450$ mm and 600 mm, there were 60 measuring points, with 5 points located on the rooftops and 55 points on the building surface. For $H_b=300$ mm and 1200 mm, the measuring points were limited to the centerline ($Y=0$ mm). For each of Case 1, Case 2 and Case 3, approximately 300 concentration measurements were obtained in the vertical centerplane.

3. RESULTS AND DISCUSSION OF WIND TUNNEL EXPERIMENTS

3.1 FLOW VISUALIZATION

Figure 4 shows the smoke flow patten for Case 3. Smoke was introduced near the base of the high-rise buildings using a Rosco 1500 smoke generator. The smoke behind the downwind building model flows upwards along the downwind face of the model. Therefore, if a source were located in the downwind wake of such a building, significant air pollution would occur there. The height of separating flow above the rooftop was slightly higher than that for Case 1.

3.2 MEAN VELOCITY CONTOURS AND STREAMLINES

Fgure 5 through 7 shows distributions of total velocity $\sqrt{U^2+W^2}$ or $\sqrt{U^2+V^2}$ and streamlines. The velocity distribution contours on a horizontal plane were plotted assuming that the flow field was symmetrical about the longitudinal centerline.

For Case 1, as shown in Figure 5, the streamlines were tightly packed near the higher levels of the downwind face. This means an eddy was created in the area. The streamlines are consistent with the results of Davies et al (1980).

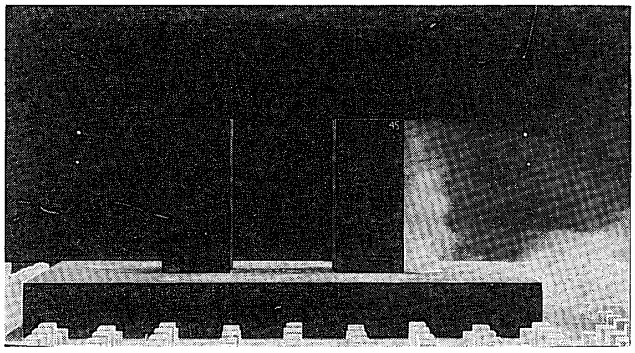

Figure 4. Smoke flow pattern fom Case 3

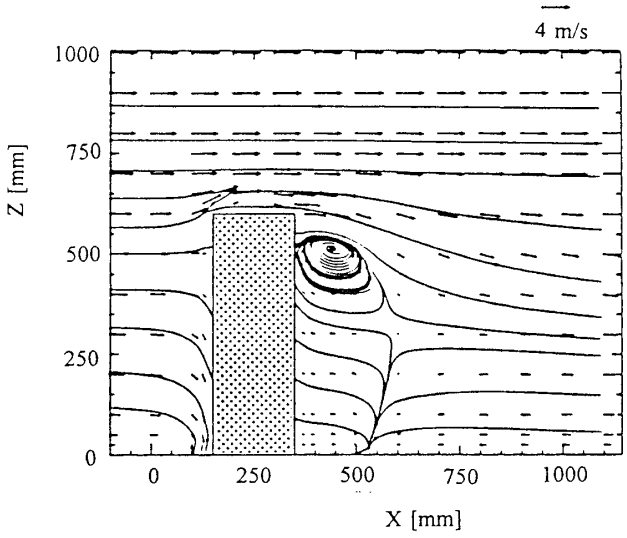

(a) Vertical centerplane ($Y=0$ mm)

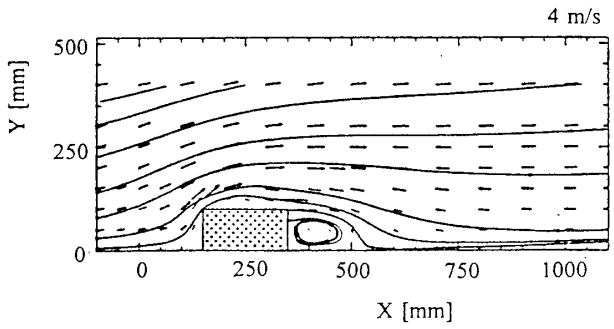

(b) Horizontal plane ($Z=50$ mm)

Figure 5. Velocity contours and streamlines for Case 1 (a) in the vertical centerplane and (b) in the horizontal plane at an elevation of 50 mm.

For Case 2, Figure 6 indicates that, in the U-W flow field, the recirculating flows appeared between the twin building models and behind the downwind building models, respectively

(Britter, 1979).

For Case 3, Figure 7 indicates that 4 eddies were created around the building models. They are located near at the upper levels of the twin high-rise buildings and at the lower level of the terrace shape building, respectively. In comparison with the flow pattern for Case 2, it was found that a larger recirculating flow was formed between the twin buildings.

3.3 BUILDING SURFACE CONCENTRATIONS

(1) EFFECT OF BUILDING CONFIGURATIONS ON CONCENTRATION DISTRRIBUTIONS

Figures 8 through 10 shows basic concentration distributions around high-rise buildings obtained while keeping the source position constant. For Case 1 with an isolated building model, the contour of $\chi=10$ on the downwind building surface occurred at a height of $Z/H_b=0.5$, and in the downstream wake, it intercepted the ground at $S/H_b=0.75$. For Case 2 with twin building models, the same contour occured at a height of $Z/H_b=0.75$ and it intercepted the ground at $S/H_b=1.05$. The diffusion region for Case 2 was larger than that for Case 1. Following Plate (1982), Figure 11 was plotted with nondimensional distance ($S'/\sqrt{A_0}$) vs. the nondimensional concentrations (χ) measured through the centerline at $Y=0$. S' is the shortest distance between the source position and the sampling port, and A_0 is the upwind face area of the upwind building model of $H_b=600$ mm. The tracer was emitted from the source of $Z=50$ mm and $S=100$ mm. The concentration profiles for Case 2 and Case 3 were shifted toward larger values of χ.

(2) EFFECT OF SOURCE POSITION ON BUILDING SURFACE CONCENTRATIONS

For Case 1 with an isolated building model,

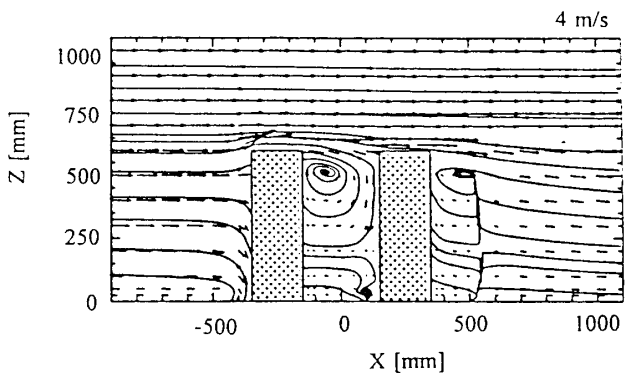

(a) Vertical centerplane (Y=0 mm)

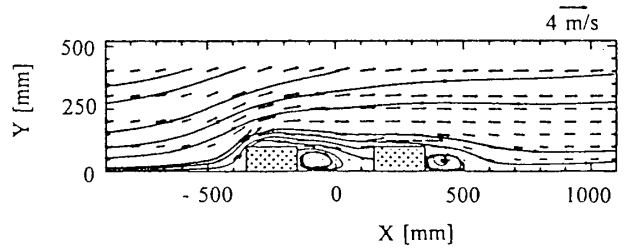

(b) Horizontal plane (Z=50 mm)

Figure 6. Velocity contours and streamlines for Case 2 (a) in the vertical centerplane and (b) in the horizontal plane at an elevation of 50 mm.

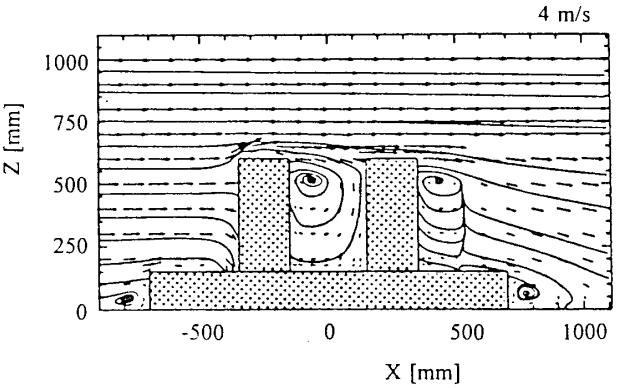

(a) Vertical centerplane (Y=0 mm)

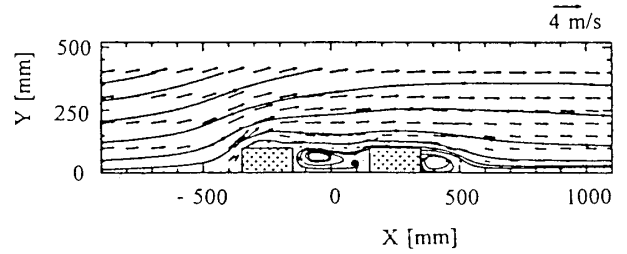

(b) Horizontal plane (Z=50 mm)

Figure 7. Velocity contours and streamlines for Case 3 (a) in the vertical centerplane and (b) in the horizontal plane at an elevation of 50 mm.

Figure 12 shows that the source elevation did not greatly affect the building surface concentrations although the maximum concentrations appeared at different elevations. This was observed for source elevations in the range of $25\ \text{mm} < Z < 100\ \text{mm}$ with the longitudinal source position constant. The following relationship between χ and $S'/\sqrt{A_0}$ exits.

$$\chi = (S'/\sqrt{A_0})^{-\alpha}$$

The α was found to have a value of 2.0.

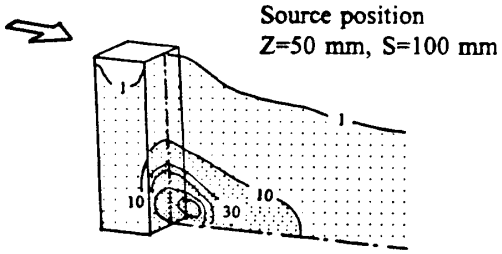

Figure 8. Concentration distributions for Case 1

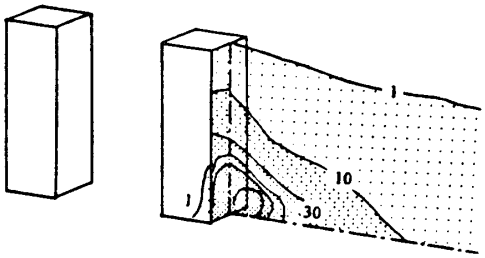

Figure 9. Concentration distributions for Case 2 in same source position as that in Figure 8.

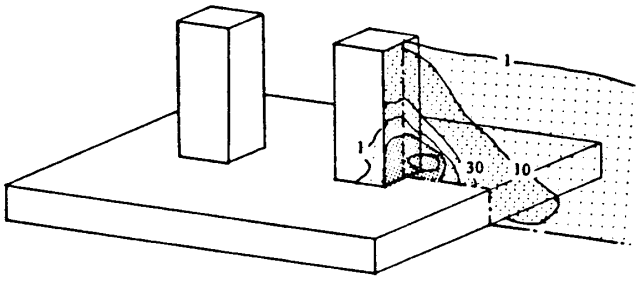

Figure 10. Concentration distributions for Case 3 in same source position as that in Figure 8.

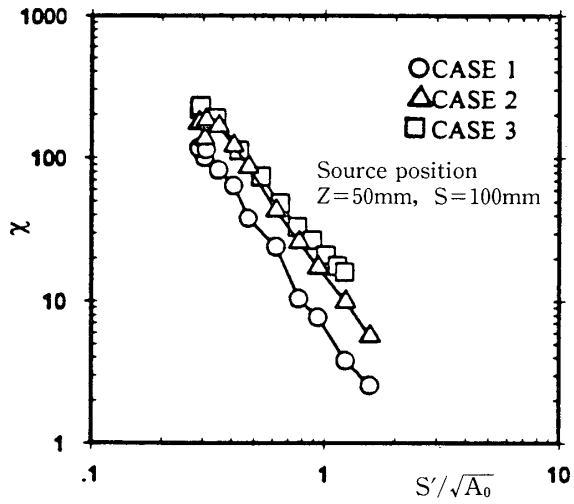

Figure 11. Effect of building configurations on building surface concentrations

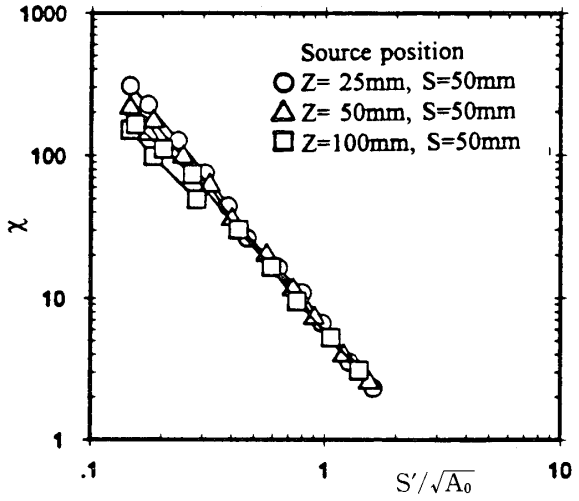

Figure 12. Effect of source positions on building downwind surface concentrations for Case 1

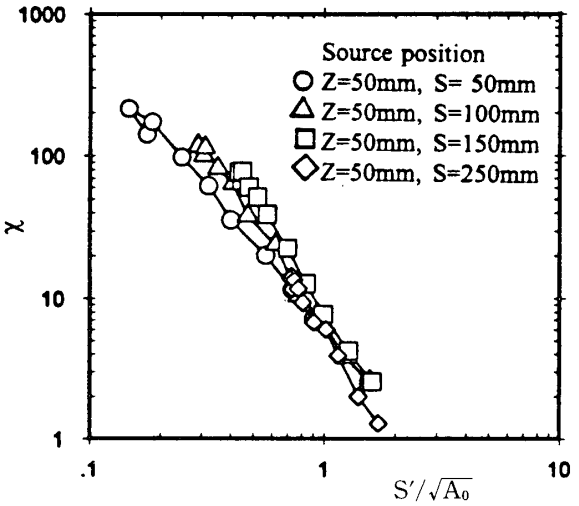

Figure 13. Effect of source positions on building surface concentrations for Case 1

Figure 13 shows the maximum concentrations decreased and the concentration curves decreased more quickly with the downstream distance S' as the source position moved downstream while keeping the source elevation constant. The α was found to vary from 2.0 to 2.8 in these cases. For Case 2 with twin building models, Figure 14 shows concentration characteristics similar to those for Case 1.

(3) EFFCT OF SEPARATION DISTANCE BETWEEN TWIN BUILDINGS ON BUILDING SURFACE CONCENTRATIONS

Figure 15 shows the effects of separation distance between twin building models on building surface concentrations. These buildings are at a height of 600 mm with terrace. In this experiment, the source positions were restricted to be located in the reverse flow region near ground level behind the downwind building model. It was found that the separation distance of the twin building models in the range of $0.25 < L/H_b < 1.0$ did not influence the downwind surface concentration profiles for the downwind building. Also, for the twin building models of $H_b = 300$ mm, 600 mm and 1200 mm without terrace, the experiments were conducted, and they showed the downwind surface concentration profiles for downwind building similar to those for Case 3, Case 4 and Case 6.

(4) EFFECT OF UPWIND FACE AREA OF BUILDING MODEL ON BUILDING SURFACE CONCENTRATIONS

Figure 16 indicates that, when the high-rise building height increased while keeping source position and separation distance between twin building models constant, the maximum concentrations were almost same among them, and the concentration profiles were shifted towards smaller values of χ.

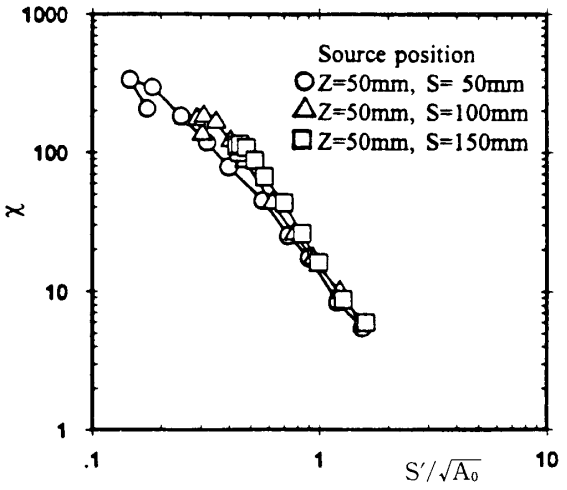

Figure 14. Effect of source positions on building surface concentrations for Case 2

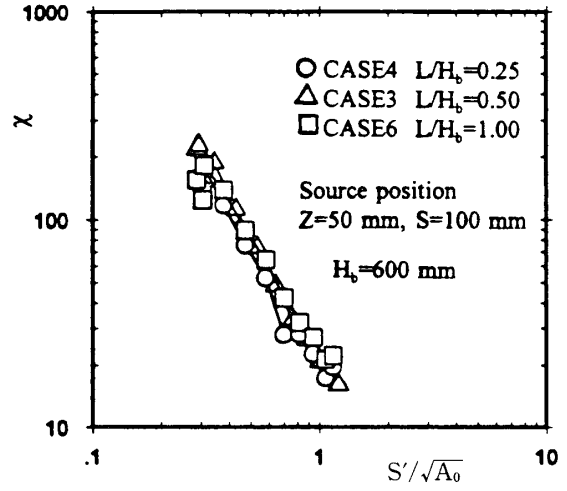

Figure 15. Effect of separation distances between twin buildings with terrace on building surface concentrations

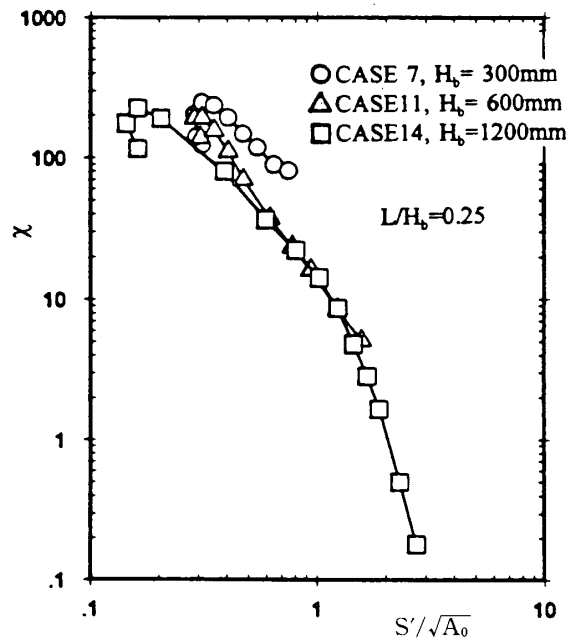

Figure 16. Effect of upwind face area of building model on building surface concentrations

4. OUTLINE OF NUMERICAL SIMULATIONS

4.1 TURBULENCE MODEL

The standard formulation for the k-ε turbulence model was used. This can simulate the incompressible turbulent flow field around a bluff body. The continuity and the Navier-Stokes equations are time-averaged and can be written as follows (Kurabuchi, 1990, Murakami, 1992) :

Continuity,

$$\frac{\partial U_i}{\partial X_i}=0$$

Transport of momentum,

$$\frac{\partial U_i}{\partial t}+U_j\frac{\partial U_i}{\partial X_j}=-\frac{\partial}{\partial X_i}\left(P+\frac{2}{3}k\right)+\frac{\partial}{\partial X_j}\left[\gamma_t\left(\frac{\partial U_i}{\partial X_j}+\frac{\partial U_j}{\partial X_i}\right)\right]$$

Tranport of turbulent kinetic energy k,

$$\frac{\partial k}{\partial t}+U_j\frac{\partial k}{\partial X_j}=\frac{\partial}{\partial X_j}\left(\frac{\gamma_t}{\sigma_1}\frac{\partial k}{\partial X_j}\right)+\gamma_t\left(\frac{\partial U_i}{\partial X_j}+\frac{\partial U_j}{\partial X_i}\right)\frac{\partial U_i}{\partial X_j}-\varepsilon$$

Transport of energy dissipation rate ε,

$$\frac{\partial \varepsilon}{\partial t}+U_j\frac{\partial \varepsilon}{\partial X_j}=\frac{\partial}{\partial X_j}\left(\frac{\gamma_t}{\sigma_2}\frac{\partial \varepsilon}{\partial X_j}\right)+\frac{\varepsilon}{k}C_1P_k-C_2\frac{\varepsilon^2}{k}$$

Transport of mean concentration C,

$$\frac{\partial C}{\partial t}+U_j\frac{\partial U}{\partial X_j}=\frac{\partial}{\partial X_j}\left(\frac{\gamma_t}{\sigma_3}\frac{\partial C}{\partial X_j}\right)$$

Here, turbulent diffusivity γ_t is

$$\gamma_t=C_D\frac{k^2}{\varepsilon}$$

Product term is

$$P_k=\gamma_t\left(\frac{\partial U_i}{\partial X_j}+\frac{\partial U_j}{\partial X_i}\right)\frac{\partial U_i}{\partial X_j}$$

$C_1=1.44$, $C_2=1.92$, $\sigma_1=1.3$, $\sigma_3=1.0$, $C_D=0.09$

4.2 GRID SYSTEM

A staggered grid system was adopted for all the simulations. Figure 17 shows a rectangular grid system of 43 cells long $\times$39 cells wide $\times$32 cells high for Case 1 with the domain dimension about 8.33 H_b long $\times$6.22 H_b wide $\times$ 3.5 H_b high where the width and height are coincident to those of the EPA wind tunnel. The smallest cell in the domain is 3/50 of the building height H_b which is 600 mm in the wind tunnel.

4.3 BOUNDARY CONDITIONS

(1) UPSTREAM BOUNDARY

The vertical profiles of velocity and turbulent kinetic energy measured in the wind tunnel, as shown in Figure 2, were used for the upstream boundary condition. The index of the power-law is 0.29. The dissipation of turbulent kinetic energy was specified by $\varepsilon=C\mu k^2/\nu_t$ where $C\mu$ is 0.09.

(2) UPPER HORIZONTAL BOUNDARY, OUTFLOW BOUNDARY AND SIDE VERTICAL BOUNDARIES

Free-slip conditions of the tangential velocity component were given, and also these normal velocity components were determined enough to satisfy the continuity equation. No-slip boundary conditions were given at the solid walls.

(3) GROUND LEVEL BOUNDARY

Assuming that boundary layer close to the ground level has a power-low index of 1/7, and the normal velocity in a dummy cell is equal to 0, the tangental velocity was given for the simulations.

(4) SOURCE CELL

The cell concentration was fixed constant assuming that the tracer gas would diffuse uniformly inside the source cell. The emission

velocity is equal to 0. Due to the limitation of grid numbers, the size of source cell was set to be much larger than that in the wind tunnel experiments. For Case 1, it is equivalent to 42 mm long×44 mm wide×36 mm high, and for Case 2 and Case 3, 60 mm long×44 mm wide×36 mm high.

4.4 NUMERICAL METHOD

The pressure-velocity relaxation of SMAC (Simplified Marker and Cell Method) was adopted for this simulation. It is equivalent to the usual SOR (Successive Over Relaxation) for the Poisson equation of the pressure field. In the simulations, the iteration number of pressure relaxation was fixed at 50 times. The CPU operation time to get stationary results of the flow took about 20 hours by a CRAY super-computer in EPA.

5. RESULTS AND DISCUSSION OF NUMERICAL SIMULATIONS

5.1 MEAN VELOCITY FIELDS

In the U-W flow field for Case 1 as shown in Figure 18, a stagnation point on the upwind face of the building model appeared at a height of $Z/H_b=2/3$. The oncoming flow flowed downwards along the upwind face and reached ground level. On the other hand, the flow separated on the upwind edge of the rooftop and reattached on the same rooftop. A reverse flow was not observed in the area near the rooftop, but a reverse flow was formed in the near-wake a little below the building height. In comparison with that in Figure 5, the reverse flow is positioned to be a little high. In the U-V flow field at Z=54 mm, the flow separated at the upwind edge of the building model and reattached on the side. A reverse flow region was also formed in the near-wake downstream

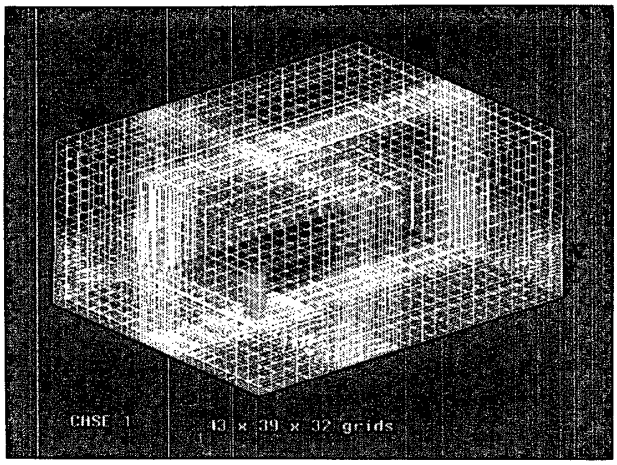

Figure 17. Finite difference grid system for Case 1

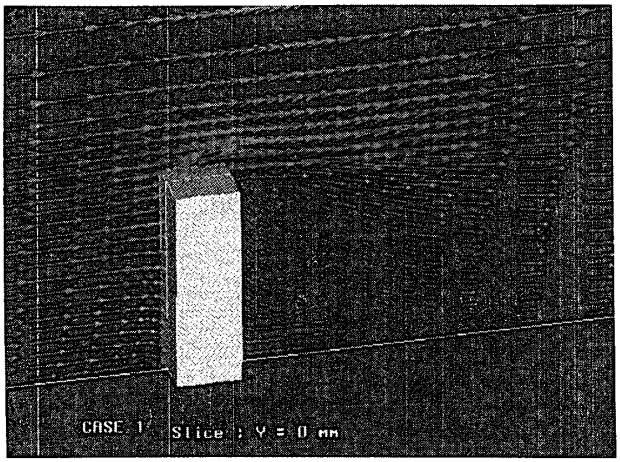

Figure 18. Velocity field in X-Z section at Y=0 mm for Case 1

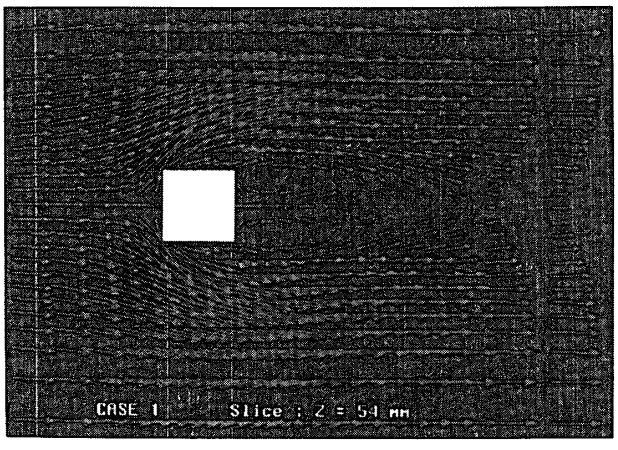

Figure 19. Velocity field in X-Y section at Z=54 mm for Case 1

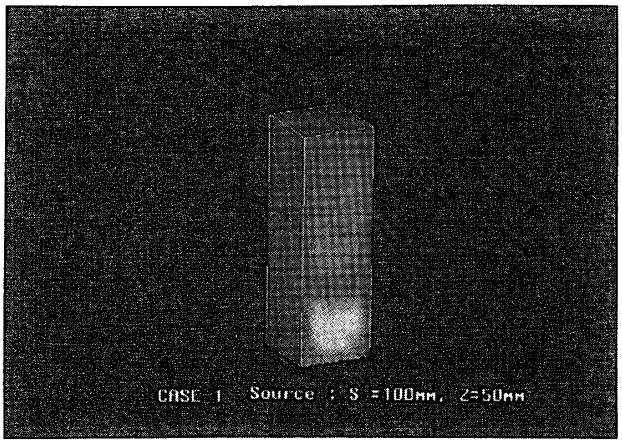

Figure 20. Building surface concentrations for Case 1

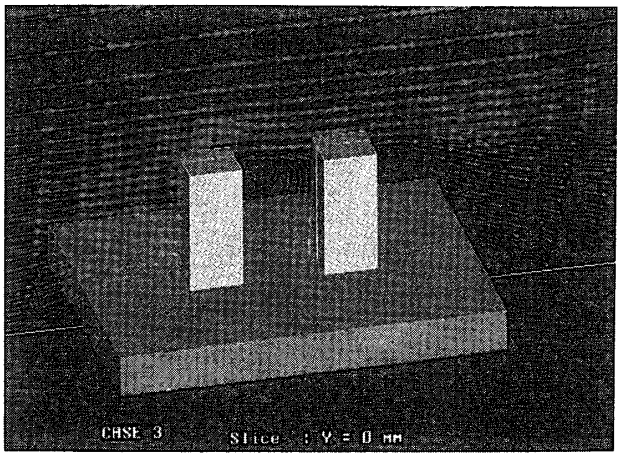

Figure 23. Velocity field in X-Z section at Y=0 mm for Case 3

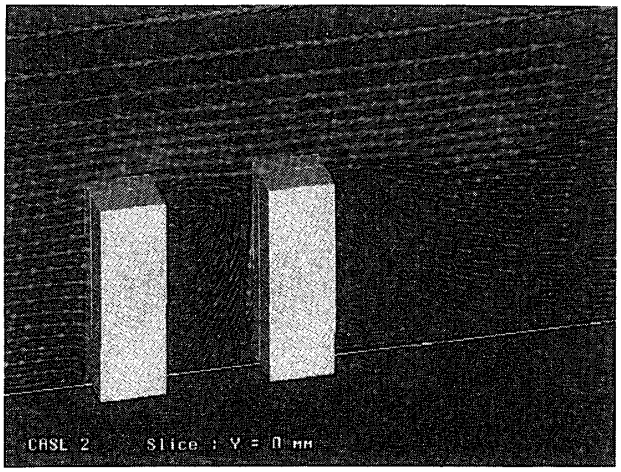

Figure 21. Velocity field in X-Z section at Y=0 mm for Case 2

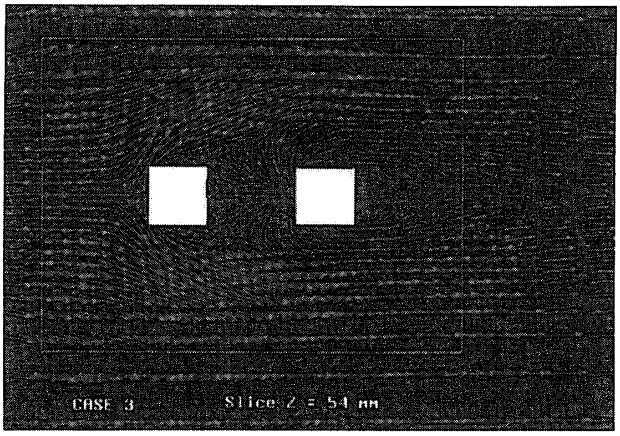

Figure 24. Veloity field in X-Y section at Z=54 mm for Case 3

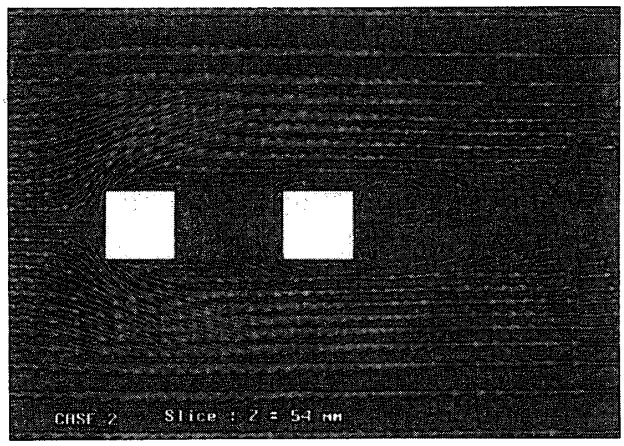

Figure 22. Velocity field in X-Y section at Z=54 mm for Case 2

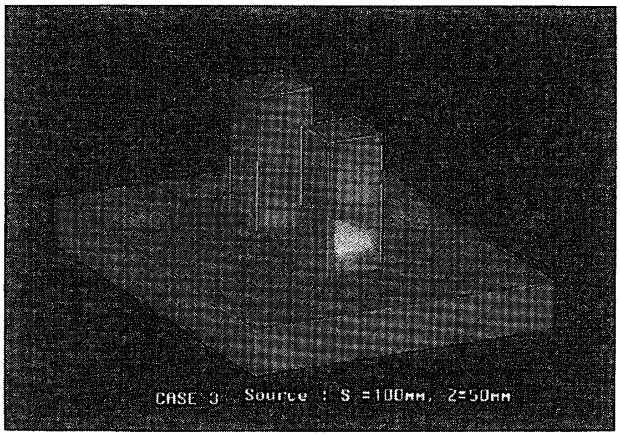

Figure 25. Building surface concentrations for Case 3

of the model. The recirculating region behind the building expands downstream of four fifth building height. This length is simulated 3.6 times longer than that in the wind tunnel data.

Next, in the U-W flow field for Case 2 as shown in Figure 21, the flow separated on the upwind rooflop edge of the upwind building model and reattached on the same rooftop. After the reattachment, the flow was directed downwards along the upwind face of the downwind building model and was directed upstream at ground level. A recirculating flow between the twin building models was not as clearly defined as that in the wind tunnel as shown in Figure 6. In the areas near the rooftop of the downwind building model, the flow was parallel to the rooftop line. A separated flow did not clearly occur on the upwind edge of the rooftop. The reverse flow region in the near-wake behind the downwind model was created. The wake length is shorter than that for Case 1.

For Case 3 in Figure 23, when a terrace-type basement was attached to the buildings for Case 2 while maintaining the building height constant, the reverse flow region between the twin buildings was formed like for Case 2. Also, small reverse flows appeared upsteam and downstream of the basement. The reverse flow region in the downwind building wake was reduced half as that for Case 1. It indicates good agreement with the wind tunnel data.

5.2 BUILDING SURFACE CONCENTRATIONS

The simulated concentrations are not displayed by the same format as those in Figure 8 through 10. Therefore, at the present stage, it is difficult to compare the results of numerical simulations with those in the wind tunnel experiments.

For Case 1 as shown in Figure 20, the maximum concentration occurred at a height of $Z/H_b = 0.12$. The position is a little lower than that in Figure 8. For Case 3, Figure 25 indicates that the maximum concentration is smaller than that for Case 1. These results are opposite to those in the wind tunnel experiments. Also, the concentration distributions are not symmetrical unlike that for Case 1. These suggest that the CPU operation time is not enough to get stationary results of the concentration field.

6. CONCLUSIONS

From these wind tunnel experiments, the following conclusions are drawn:

(1) The three-dimensional velocity vectors around the high-rise building models were measured precisely using the pulsed wire anemometer. A recirculating eddy was observed in the mean flow field just downstream and near the top of the high-rise building models.

(2) Provided the twin building models were located such that $L/H_b > 1.0$, then the upwind building would reduce the effects on the flow fields near the top of the downwind building model.

(3) In comparison with the building surface concentrations and concentration profiles downstream of the isolated building model, the twin building models caused higher concentrations in the near-wake behind the downwind building model.

(4) When the source positions were restricted to the downwind building wake of the twin building models, the source elevation did not strongly influence the building surface concentration distributions although the maximum concentrations appeared at different elevations. However, when the source was moved downstream while maintaining the source height constant, the maximum concentration de-

creased and the concentration curve decreased more sharply with the distance between the source position and the sampling port.

(5) Variation of the separation distance between the twin building models in the range of $0.25 < L/H_b < 1.0$ did not substantially affect the magnitude of the downwind surface concentration contours for the downwind building.

(6) When the face area of upwind building model increased, the concentrations on the downwind face of the downwind building model for the twin building models decreased for the same distance between the source position and the sampling port on the building model.

Also, from the numerical simulations, the following conclusions are dawn:

(1) The mean flow fields for the twin high-rise building models with a terrace-type basement have reasonable ageement with the wind tunnel data.

(2) But, for a single high-rise building model, the length of recirculating flow behind the building model was predicted 3 times longer than that in the wind tunnel experiments. It caused the downwind building surface concentrations in a single high-rise building model higher than those in the twin high-rise building models.

Our k-ε model can not succeed to predict accurately the complex flow field around the high-rise building models. Afterwards, we would like to investigate precisely the incoincidence between the results of wind tunnel experiments and those of numerical simulations, and improve the accuracy of the k-ε model.

REFERENCES

Snyder, W. H. 1979 The EPA Meteorological Wind Tunnel: Its Design, Construction, and Operating Characteristics. Rpt. No. EPA-600/4-79-051, Envir. Prot. Agcy., Res., Tri. PK., NC, 78p.

Irwin, H. P. A. H. 1981 The Design of Spires for Wind Simulation. J. Wind Engr. Indus. Aerodyn., **7**, 361-366.

Davies, M. E., Quincey, V. C. & Tindall, S. J. 1980 The Near-Wake of a Tall Building Block in Uniform and Turbulent Flows. Proc. 5th Int. Conf. Wind Enger., Fort Collins, Co, July, 1979 (J. E. Cermak, ed.), V. 1, p.289-98. Pergamon Press, NY, NY.

Britter, R. E. & Hunt, J. C. R. 1979 Velocity Measurements and Order of Magnitude Estimates of the Flow Between Two Buildings in a Simulated Atmospheric Boundary Layer, J. Indus. Aerodyn., 4, 165-182.

Plate, E. 1982 Engineering Meteorology, Elsevier Scientific Pub., 496-497.

Kurabuchi, T., Fang, J. B. & Grot, R. A., 1990 A Numerical Method For Calculating Indoor Airflows Using a Turbulence Model. NISTIR 89-4211.

Murakami, S. 1992 Comparison of various turbulence models applied to a bluff body, J. of Wind Engineering, No. 52, 164-179.

Lawson, R. E., Jr. and Ohba, M. 1993 Physical Modeling of the Flow Field Around Twin High-Rise Buildings. AMS Eighth Joint Conf. On Applications of Air Pollution Meteorology, Jan 23-28, Nashville, TN.

Ohba, M and Lawson, R. E., Jr. 1993 Physical Modeling of Concentration Distributions Around Twin High-Rise Buildings With a District Heating Plant. AMS Eighth Joint Conf. On Applications of Air Pollution Meteorology, Jan 23-28, Nashville, TN.